

Salicylaldoxime in manganese(III) carboxylate chemistry: Synthesis, structural characterization and physical studies of hexanuclear and polymeric complexes

Catherine P. Raptopoulou^{a,*}, Athanassios K. Boudalis^{a,*}, Katerina N. Lazarou^a, Vassilis Psycharis^a, Nikos Panopoulos^a, Michael Fardis^a, George Diamantopoulos^a, Jean-Pierre Tuchagues^b, Alain Mari^b, George Papavassiliou^a

^aInstitute of Materials Science, NCSR "Demokritos", 15310 Aghia Paraskevi, Athens, Greece

^bLaboratoire de Chimie de Coordination du CNRS, UPR 8241, 205 Route de Narbonne, 31077 Toulouse, France

ARTICLE INFO

Article history:

Received 15 July 2008

Accepted 31 August 2008

Available online 8 October 2008

Keywords:

Manganese(III) clusters

Hexanuclear complexes

Polymeric complexes

Magnetic studies

Salicylaldoxime

ABSTRACT

The use of salicylaldehyde oxime (H₂salox) in manganese(III) carboxylate chemistry has yielded new members of the family of hexanuclear compounds presenting the [Mn₆(μ₃-O)₂(μ₂-OR)₂]¹²⁺ core, complexes [Mn₆^{III}(μ₃-O)₂(O₂CPh)₂(salox)₆(L₁)₂(L₂)₂] (L₁ = py, L₂ = H₂O (**1**); L₁ = Me₂CO, L₂ = H₂O (**2**); L₁ = L₂ = MeOH (**3**)). Addition of NaOMe to the acetonitrile reaction mixture, afforded the 1D complex [Mn₃^{III}Na(μ₃-O)(O₂CPh)₂(salox)₃(MeCN)]_n (**4**), whereas addition of NaClO₄ to the acetone reaction mixture afforded an analogous 1D complex [Mn₃^{III}Na(μ₃-O)(O₂CPh)₂(salox)₃(Me₂CO)]_n (**5**). The structures of **1–3** present the [Mn₆(μ₃-O)₂(μ₂-OR)₂]¹²⁺ core and can be described as two [Mn₃(μ₃-O)]⁷⁺ triangular subunits linked by two μ₂-oximate oxygen atoms of the salox²⁻ ligands, which show the less common μ₃-κ²O:κO':κN coordination mode. The benzoato ligands are coordinated through the usual *syn,syn*-μ₂-κO:κO' mode. The 1D polymeric structures of **4** and **5** consist of alternating [Mn₃(μ₃-O)]⁷⁺ subunits and Na⁺ atoms linked through two μ₃-κ²O:κO':κN and one μ₄-κ²O:κ²O':κN salox²⁻ ligands as well as one *syn,anti*-μ₂-κO:κO' benzoato ligand. DC and AC magnetic susceptibility studies on **1** revealed the stabilization of an S = 4 ground state, and indications of single-molecule magnetism behavior, whereas the DC experimental data from polycrystalline sample of **5** are indicative of antiferromagnetic interactions within the [Mn₃] subunit. Solid state ¹H NMR data of **1** were used to probe the spin-lattice relaxation of the system.

© 2008 Elsevier Ltd. All rights reserved.

1. Introduction

Polynuclear homo- and/or hetero-metallic transition metal complexes (clusters) stand in the heart of modern inorganic chemistry research mainly due to their biomimetic [1] and physical properties [2] which are closely related to their structural characteristics. In most of the cases, the synthesis of the clusters is governed by self-assembly principles [3]. The labile nature of the coordination bonds, among other parameters, such as the crystallization process (which is governed by weak H-bonding, π–π stacking and Van der Waals interactions), the nature of the ligands and the coordinative flexibility of metal ions and ligands constitute some of the features that make this chemistry so difficult to control. However, during the last 15 years a great progress has been made on the rational synthesis of metal clusters either by the chemical modification of accidentally preformed clusters [4] or

by the proper use of oligonuclear precursors [5] ('building blocks') and/or specially designed ligands [6].

Our research efforts are mainly oriented towards the study of the physical properties of clusters prepared either accidentally in the realm of self-assembly [7] or under more 'sophisticated' rational synthetic approaches [8]. Our research interests include also, the investigation of the effect of various key factors, like ligand substitution [9], solvent [10], crystallization method [11], as well as reactivity of metal clusters [12]. The work presented herein, constitutes part of our research project on oximate complexes [8a,10,12,13], and in particular on complexes containing salicylaldehyde oxime (H₂salox) as ligand. Our previous experience on the Fe^{III}/H₂salox/PhCO₂⁻ reaction system revealed that, depending on the reaction solvent, trinuclear [10] or hexanuclear [8a] complexes were isolated. Initial results concerning the Mn^{III}/H₂salox/RCO₂⁻ (R = Me, Ph) reaction system have been reported by Perlepes and his coworkers [14]. We present herein, the investigation of various reaction parameters, such as the reaction solvent (MeCN, Me₂CO, MeOH), the presence of externally added base and/or counterions, the use of oligonuclear manganese clusters as starting materials, the stoichiometry of the reactants and the crystallization method,

* Corresponding authors. Tel.: +30 210 6503346; fax: +30 210 6519430 (C.P. Raptopoulou).

E-mail addresses: craptop@ims.demokritos.gr (C.P. Raptopoulou), tbou@ims.demokritos.gr (A.K. Boudalis).

to the identity of the $\text{Mn}^{\text{III}}/\text{H}_2\text{salox}/\text{RCO}_2^-$ ($\text{R} = \text{Ph}$) reaction system, i.e. the synthesis, structural and physical properties studies of the hexanuclear complexes $[\text{Mn}_6^{\text{III}}(\mu_3\text{-O})_2(\text{O}_2\text{CPh})_2(\text{salox})_6(\text{L}_1)_2(\text{L}_2)_2] \cdot x\text{MeCN} \cdot y\text{MeOH} \cdot z\text{H}_2\text{O} \cdot w\text{Me}_2\text{CO}$ ($\text{L}_1 = \text{py}$, $\text{L}_2 = \text{H}_2\text{O}$, $x = 6$, $y = 0$, $z = 0$, $w = 0$ (**1**); $\text{L}_1 = \text{Me}_2\text{CO}$, $\text{L}_2 = \text{H}_2\text{O}$, $x = 0$, $y = 0$, $z = 0$, $w = 2$ (**2**); $\text{L}_1 = \text{L}_2 = \text{MeOH}$, $x = 0$, $y = 1$, $z = 0.5$, $w = 0$ (**3**)) and the 1D complexes $[\text{Mn}_3^{\text{III}}\text{Na}(\mu_3\text{-O})(\text{O}_2\text{CPh})_2(\text{salox})_3(\text{S})]_n \cdot n\text{S}$ ($\text{S} = \text{MeCN}$ (**4**); $\text{S} = \text{Me}_2\text{CO}$ (**5**)).

2. Experimental

2.1. General and spectroscopic measurements

All manipulations were performed under aerobic conditions using materials as received (Aldrich Co). All chemicals and solvents were of reagent grade. $[\text{Mn}_2^{\text{III}}\text{Mn}^{\text{II}}(\mu_3\text{-O})(\text{O}_2\text{CPh})_6(\text{py})_2(\text{H}_2\text{O})]$ [**15**] and $(\text{NBu}^n)_4[\text{Mn}_4^{\text{III}}\text{O}_2(\text{O}_2\text{CPh})_9(\text{H}_2\text{O})]$ [**16**] were synthesized as previously described. Elemental analysis for carbon, hydrogen, and nitrogen was performed on a Perkin Elmer 2400/II automatic analyzer. Infrared spectra were recorded as KBr pellets in the range 4000–400 cm^{-1} on a Bruker Equinox 55/S FT-IR spectrophotometer. Variable-temperature magnetic susceptibility measurements were carried out on polycrystalline samples of **1** and **5** using a Quantum Design MPMS SQUID susceptometer. DC data were collected in the 2–300 K temperature range under magnetic fields of 0.1, 0.5, 1, 2.5 and 5 T for **1** and under a field of 0.5 T for **5**. AC data for **1** were collected between 2 and 7.5 K, with an oscillating field of 1 G amplitude oscillating at frequencies of 0.1, 1, 10, 33, 99.9, 332, 997, 1400 Hz. Diamagnetic corrections for the complexes were estimated from Pascal's constants. The magnetic susceptibility of **5** has been computed by exact calculation of the energy levels associated with the spin Hamiltonian through diagonalization of the full matrix with a general program for axial symmetry [**17**]. Least-squares fittings were accomplished with an adapted version of the function-minimization program MINUIT [**18**]. The error factor R is defined as $R = \sum \frac{(x_{\text{exp}} - x_{\text{calc}})^2}{N x_{\text{exp}}^2}$, where N is the number of experimental points. ^1H pulsed NMR experiments on polycrystalline sample of **1** were performed at 2.4 T using a coherent spectrometer operating at 2.4 T (100 MHz for ^1H NMR). An Oxford 1200 CF continuous flow cryostat was employed for measurements in the range 5–300 K. The T_1 spin-lattice relaxation time was obtained using the standard saturation technique [**19**].

2.2. Compound preparations

2.2.1. $[\text{Mn}_6^{\text{III}}(\mu_3\text{-O})_2(\text{O}_2\text{CPh})_2(\text{salox})_6(\text{py})_2(\text{H}_2\text{O})_2] \cdot 6\text{MeCN}$ (**1** · 6MeCN)

2.2.1.1. Method A. Solid H_2salox (0.014 g, 0.10 mmol) was added to a red brown solution of $[\text{Mn}_3(\mu_3\text{-O})(\text{O}_2\text{CPh})_6(\text{py})_2(\text{H}_2\text{O})]$ (0.108 g, 0.10 mmol) in MeCN (30 mL) and the resulting brown solution was refluxed for 1 h. Small portions of an orange-brown precipitate were filtered off, and the brown filtrate was left for slow evaporation. After 5 days, a mixture of green-brown prismatic crystals of **1** and orange cubic crystals were formed. The latter identified as the mixed-valence hexanuclear complex $[\text{Mn}^{\text{II}}_4\text{Mn}^{\text{III}}_2(\mu_4\text{-O})_2(\text{O}_2\text{CPh})_{10}(\text{py})_2(\text{H}_2\text{O})(\text{MeCN})] \cdot 2\text{MeCN}$ by unit cell determination [**20**].

2.2.1.2. Method B. Solid H_2salox (0.069 g, 0.50 mmol) was added to a red brown solution of $[\text{Mn}_3(\mu_3\text{-O})(\text{O}_2\text{CPh})_6(\text{py})_2(\text{H}_2\text{O})]$ (0.184 g, 0.17 mmol) in MeCN (50 mL) and the resulting brown solution was refluxed for 1 h. The brown solution was left for slow evaporation and after 20 days green-brown prismatic crystals of **1** were formed, which were filtered off, washed with cold MeCN and dried *in vacuo* (yield: 0.093 g, 67% based on the metal). The resulting powder was analyzed as solvent free. $\text{C}_{66}\text{H}_{54}\text{Mn}_6\text{N}_8\text{O}_{20}$ requires:

C, 49.27; H, 3.38; N, 6.96. Found: C, 49.02; H, 3.36; N, 6.93%. FT-IR (KBr pellets, cm^{-1}): 3450(br), 3054(w), 3013(w), 2927(w), 1598(vs), 1529(vs), 1472(m), 1440(vs), 1394(vs), 1358(w), 1324(m), 1283(vs), 1200(m), 1154(m), 1126(m), 1068(w), 1043(s), 1027(vs), 1009(m), 961(w), 918(s), 851(w), 826(m), 754(s), 721(s), 678(vs), 652(m), 625(w), 530(w), 472(m).

2.2.2. $[\text{Mn}_6^{\text{III}}(\mu_3\text{-O})_2(\text{O}_2\text{CPh})_2(\text{salox})_6(\text{Me}_2\text{CO})_2(\text{H}_2\text{O})_2] \cdot 2\text{Me}_2\text{CO}$ (**2** · 2Me₂CO)

2.2.2.1. Method A. Solid H_2salox (0.034 g, 0.25 mmol) was added to a refluxed red brown solution of $[\text{Mn}_3(\mu_3\text{-O})(\text{O}_2\text{CPh})_6(\text{py})_2(\text{H}_2\text{O})]$ (0.092 g, 0.085 mmol) in Me_2CO (30 mL) and the resulting brown solution was further refluxed for 15 min. Vapor diffusion of Et_2O to the brown reaction mixture afforded X-ray quality brown needle-like crystals of **2**, which were filtered off, and dried *in vacuo* (yield: 0.040 g, 60% based on the metal). The resulting powder was analyzed as solvent free. $\text{C}_{62}\text{H}_{56}\text{Mn}_6\text{N}_6\text{O}_{22}$ requires: C, 47.53; H, 3.60; N, 5.36. Found: C, 47.29; H, 3.57; N, 5.33%. FT-IR (KBr pellets, cm^{-1}): 3410(br), 3056(w), 3015(w), 1701(m), 1634(sh), 1597(vs), 1536(vs), 1472(s), 1440(vs), 1396(vs), 1327(m), 1282(vs), 1202(s), 1152(m), 1125(m), 1044(vs), 1028(vs), 956(w), 917(vs), 856(w), 825(m), 755(s), 722(s), 676(vs), 648(s), 550(w), 531(m), 465(s).

2.2.2.2. Method B. Solid H_2salox (0.034 g, 0.25 mmol) and solid NaOMe (0.027 g, 0.50 mmol) were added to a refluxed red brown solution of $[\text{Mn}_3(\mu_3\text{-O})(\text{O}_2\text{CPh})_6(\text{py})_2(\text{H}_2\text{O})]$ (0.092 g, 0.085 mmol) in Me_2CO (30 mL) and the resulting brown solution was further refluxed for 20 min. Small portions of a white precipitate (probably insoluble NaOMe) were filtered off, and the brown filtrate was layered with $\text{Et}_2\text{O}/n\text{-hex}$ to afford brown crystals, which were filtered off and dried *in vacuo* (yield: 0.043 g, 65% based on the metal). The brown crystals were identified as compound **2** · 2Me₂CO by unit cell determination ($a = 32.948(1)$, $b = 32.948(1)$, $c = 14.381(1)$ Å, $V = 15611.6(2)$ Å³, see Table 1).

2.2.3. $[\text{Mn}_6^{\text{III}}(\mu_3\text{-O})_2(\text{O}_2\text{CPh})_2(\text{salox})_6(\text{MeOH})_4] \cdot \text{MeOH} \cdot 0.5\text{H}_2\text{O}$ (**3** · MeOH · 0.5H₂O)

Solid H_2salox (0.034 g, 0.25 mmol) and solid MeONa (0.027 g, 0.50 mmol) were added to a red brown solution of $[\text{Mn}_3(\mu_3\text{-O})(\text{O}_2\text{CPh})_6(\text{py})_2(\text{H}_2\text{O})]$ (0.092 g, 0.085 mmol) in MeOH (30 mL) and the resulting green-brown solution was refluxed for half hour, upon which time the solution turned to brown. Small portions of a dark brown precipitate were filtered off, and the brown filtrate was left for slow evaporation. After a period of one month, brown prismatic crystals of **3** were formed, which were filtered off, washed with cold MeOH and dried *in vacuo* (yield: 0.039 g, 60% based on the metal). The resulting powder was analyzed as solvent free. $\text{C}_{60}\text{H}_{56}\text{Mn}_6\text{N}_6\text{O}_{22}$ requires: C, 46.71; H, 3.66; N, 5.45. Found: C, 46.47; H, 3.63; N, 5.42%. FT-IR (KBr pellets, cm^{-1}): 3420(br), 3052(w), 3011(w), 2926(w), 1597(vs), 1527(vs), 1471(m), 1440(vs), 1393(vs), 1358(w), 1322(m), 1282(vs), 1200(m), 1154(m), 1126(m), 1067(w), 1042(s), 1027(vs), 1009(m), 960(w), 918(s), 851(w), 826(m), 755(s), 722(s), 679(vs), 652(m), 625(w), 531(w), 474(m).

2.2.4. $[\text{Mn}_3^{\text{III}}\text{Na}(\mu_3\text{-O})(\text{O}_2\text{CPh})_2(\text{salox})_3(\text{MeCN})]_n \cdot n\text{MeCN}$ (**4** · nMeCN)

2.2.4.1. Method A. Solid H_2salox (0.034 g, 0.25 mmol) and solid NaOMe (0.027 g, 0.50 mmol) were added to a refluxed red-brown solution of $[\text{Mn}_3(\mu_3\text{-O})(\text{O}_2\text{CPh})_6(\text{py})_2(\text{H}_2\text{O})]$ (0.092 g, 0.085 mmol) in MeCN (30 mL), and the resulting brown solution was further refluxed for half hour. Small portions of a white precipitate (probably insoluble NaOMe) were filtered off, and the brown filtrate was left undisturbed in closed vials. After one week X-ray quality brown needle-like crystals were formed, which were filtered off and dried *in vacuo* (yield: 0.053 g, 70% based on the metal). The resulting

Table 1Crystallographic data for complexes **1** · 6MeCN, **2** · 2Me₂CO, **3** · MeOH · 0.5H₂O, **4** · nMeCN and **5** · nMe₂CO

	1 · 6MeCN	2 · 2Me ₂ CO	3 · MeOH · 0.5H ₂ O	4 · nMeCN	5 · nMe ₂ CO
Formula	C ₇₈ H ₇₂ Mn ₆ N ₁₄ O ₂₀	C ₆₈ H ₆₈ Mn ₆ N ₆ O ₂₄	C ₆₁ H ₆₁ Mn ₆ N ₆ O _{23.5}	C ₃₉ H ₃₁ Mn ₃ N ₅ NaO ₁₁	C ₄₁ H ₃₇ Mn ₃ N ₃ NaO ₁₃
Fw	1855.14	1682.92	1583.80	933.50	967.56
Space group	P1	I4 ₁ /a	P1	P2 ₁ /c	P2 ₁ /c
T (°C)	25	25	−170	25	25
λ (Å)	Mo Kα (0.71073 Å)	Cu Kα (1.54187 Å)	Mo Kα (0.71069 Å)	Cu Kα (1.54187 Å)	Mo Kα (0.71069 Å)
a (Å)	12.588(7)	32.8892(6)	12.797(1)	14.5372(3)	15.2662(9)
b (Å)	12.841(7)	32.8892(6)	14.146(2)	17.6493(3)	17.8828(10)
c (Å)	13.438(7)	14.3012(3)	19.830(2)	16.1490(3)	16.1926(10)
α (°)	77.16(2)		86.310(3)		
β (°)	77.89(2)		69.983(3)	108.2725(7)	93.456(2)
γ (°)	87.81(2)		81.465(3)		
V Å ³	2070.6(2)	15469.6(5)	3335.2(7)	3934.5(1)	4412.6(5)
Z	1	8	2	4	4
ρ _{calc} (g cm ^{−3})	1.488	1.445	1.577	1.576	1.456
μ (mm ^{−1})	0.965 (Mo Kα)	8.382 (Cu Kα)	1.184 (Mo Kα)	8.405 (Cu Kα)	0.920 (Mo Kα)
R ₁ ^a	0.0660 ^b	0.0475 ^c	0.0773 ^d	0.0524 ^e	0.0972 ^f
wR ₂ ^a	0.1769 ^b	0.1236 ^c	0.1938 ^d	0.0969 ^e	0.2270 ^f

^a $w = 1/[\sigma^2(F_o^2) + (aP)^2 + bP]$ and $P = (\max(F_o^2, 0) + 2F_c^2)/3$; $R_1 = \sum(|F_o| - |F_c|)/\sum|F_o|$ and $wR_2 = \{\sum[w(F_o^2 - F_c^2)^2]/\sum[w(F_o^2)^2]\}^{1/2}$.

^b For 5740 reflections with $I > 2\sigma(I)$.

^c For 4251 reflections with $I > 2\sigma(I)$.

^d For 6754 reflections with $I > 2\sigma(I)$.

^e For 5301 reflections with $I > 2\sigma(I)$.

^f For 3739 reflections with $I > 2\sigma(I)$.

powder was analyzed as solvent free. C₃₇H₂₈Mn₃N₄NaO₁₁ requires: C, 49.80; H, 3.16; N, 6.28. Found: C, 49.55; H, 3.14; N, 6.24%. FT-IR (KBr pellets, cm^{−1}): 3428(br), 3056(w), 3012(w), 2927(w), 1654(s), 1596(vs), 1534(vs), 1473(s), 1440(vs), 1394(vs), 1367(s), 1322(m), 1277(vs), 1203(s), 1152(m), 1121(m), 1105(w), 1067(w), 1040(sh), 1022(vs), 957(w), 916(vs), 853(w), 825(m), 758(s), 720(s), 707(s), 672(vs), 653(sh), 551(w), 531(m), 478(m), 462(s).

2.2.4.2. Method B. Solid H₂salox (0.014 g, 0.10 mmol) and solid NaClO₄ · H₂O (0.028 g, 0.20 mmol) were added to a red-brown solution of (NBuⁿ)₄[Mn₄O₂(O₂CPh)₉(H₂O)] (0.040 g, 0.025 mmol) in MeCN (30 mL). The resulting brown solution was refluxed for 45 min. Layer of Et₂O to the brown reaction mixture afforded X-ray quality brown crystals which were filtered off and dried *in vacuo* (yield: 0.014 g, 63% based on the metal). The brown crystals were identified as compound **4** · nMeCN by unit cell determination ($a = 14.554(2)$, $b = 17.670(3)$, $c = 16.168(3)$ Å, $\beta = 108.258(6)^\circ$, $V = 3948.6(2)$ Å³, see Table 1).

2.2.5. [Mn^{III}Na(μ₃-O)(O₂CPh)₂(salox)₃(Me₂CO)]_n · nMe₂CO (5 · nMe₂CO)

Solid H₂salox (0.014 g, 0.10 mmol) and solid NaClO₄ · H₂O (0.028 g, 0.20 mmol) were added to a red-brown solution of (NBuⁿ)₄[Mn₄O₂(O₂CPh)₉(H₂O)] (0.040 g, 0.025 mmol) in Me₂CO (30 mL). The resulting brown solution was refluxed for 45 min. Layering or vapor diffusion of Et₂O or Et₂O/n-hex to the brown reaction mixture afforded X-ray quality brown crystals which were filtered off and dried *in vacuo* (yield: 0.024 g, 74% based on the metal). The resulting powder was analyzed as solvent free. C₄₁H₃₇Mn₃N₃NaO₁₃ requires: C, 50.90; H, 3.86; N, 4.34. Found: C, 50.64; H, 3.84; N, 4.31. FT-IR (KBr pellets, cm^{−1}): 3422(br), 3057(w), 3011(w), 2930(w), 1705(m), 1652(s), 1595(vs), 1537(vs), 1472(s), 1440(vs), 1395(vs), 1365(s), 1323(m), 1278(vs), 1204(s), 1154(m), 1123(m), 1106(w), 1069(w), 1040(sh), 1024(vs), 959(w), 917(vs), 854(w), 826(m), 759(s), 721(s), 706(s), 673(vs), 653(sh), 550(w), 531(m), 478(m), 462(s).

2.3. Single-crystal X-ray crystallography

A green-brown prismatic crystal of **1** (0.18 × 0.36 × 0.70 mm) was mounted in capillary. Diffraction measurements were made

on a Crystal Logic Dual Goniometer diffractometer using graphite-monochromated Mo Kα radiation. Unit cell dimensions were determined and refined by using the angular settings of 25 automatically centred reflections in the range 11° < 2θ < 23°. Three standard reflections monitored every 97 reflections showed less than 3% intensity fluctuation and no decay. Lorentz, polarization corrections were applied using Crystal Logic software. Brown crystals of **2** (0.08 × 0.12 × 0.60 mm), **4** (0.08 × 0.25 × 0.25 mm), and **5** (0.08 × 0.55 × 0.65 mm) were mounted in capillaries with drops of mother liquor. A brown crystal of **3** (0.09 × 0.09 × 0.19 mm) was taken directly from the mother liquor and immediately cooled to −170 °C. Diffraction measurements for **2–5** were made on a Rigaku R-Axis SPIDER Image Plate diffractometer using graphite monochromated Mo Kα (**3, 5**) and Cu Kα radiation (**2, 4**). Data collection (ω-scans) and processing (cell refinement, data reduction and empirical absorption correction) were performed using the CRYSTALCLEAR program package [21]. Important crystal data and parameters for data collection are reported in Table 1. The structures were solved by direct methods using SHELXS-97 [22] and refined by full matrix least-squares techniques on F² with SHELXL-97 [23]. Further experimental crystallographic details for **1**: 2θ_{max} = 50°; reflections collected/unique/used, 7648/7276 [R_{int} = 0.0217]/7276; 611 parameters refined; (Δ/σ)_{max} = 0.004; (Δρ)_{max}/(Δρ)_{min} = 1.192/−0.1409 e/Å³; R/R_w (for all data), 0.0830/0.1955. Hydrogen atoms were located by difference maps and were refined isotropically, except those of the coordinated pyridine and the solvate molecules which were introduced at calculated positions as riding on bonded atoms. All non-H atoms were refined anisotropically. The crystals of **2** were very thin needles. Repeating efforts to increase their size proved unsuccessful. Data were collected to 2θ_{max} = 144° but only those to 2θ_{max} = 125° were used for the refinement, since in greater θ values more than 50% of the collected data were unobserved. Further experimental crystallographic details for **2**: 2θ_{max} = 125°; reflections collected/unique/used, 31770/5864 [R_{int} = 0.0491]/5864; 557 parameters refined; (Δ/σ)_{max} = 0.008; (Δρ)_{max}/(Δρ)_{min} = 0.564/−0.341 e/Å³; R/R_w (for all data), 0.0758/0.1423. Hydrogen atoms were located by difference maps and were refined isotropically, except those of the methyl groups which were introduced at calculated positions as riding on bonded atoms. All non-H atoms were refined anisotropically. The crystals of **3** were very small in size. Repeating efforts to increase their size proved un-

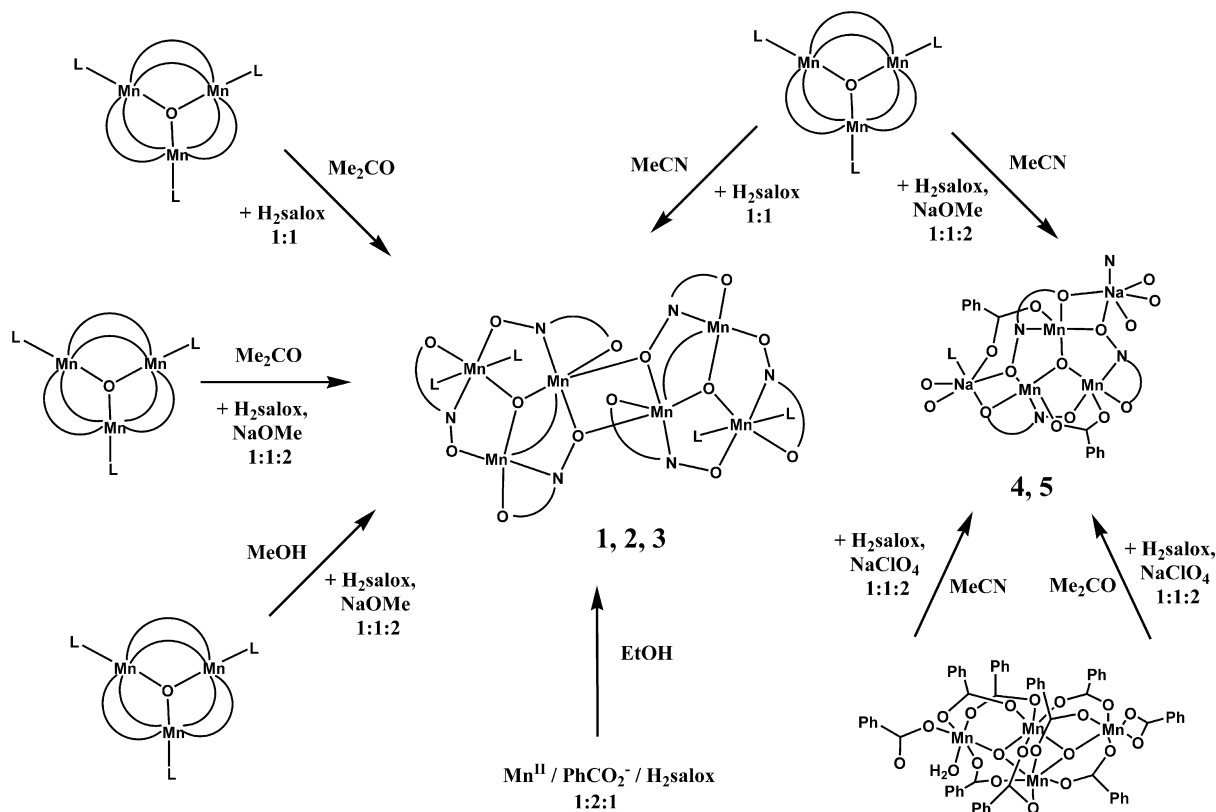
cessful. Data were collected to $2\theta_{\max} = 55^\circ$ but only those to $2\theta_{\max} = 46.5^\circ$ were used for the refinement, since in greater θ values more than 50% of the collected data were unobserved. Further experimental crystallographic details for **3**: reflections collected/unique/used, 19418/9471 [$R_{\text{int}} = 0.0684$]/9471; 884 parameters refined; $(\Delta/\sigma)_{\max} = 0.007$; $(\Delta\rho)_{\max}/(\Delta\rho)_{\min} = 0.847/-0.673 \text{ e}/\text{\AA}^3$; R/R_w (for all data), 0.1034/0.2107. Hydrogen atoms were introduced at calculated positions as riding on bonded atoms; no H-atoms for the water solvate molecule were included in the refinement. All non-H atoms were refined anisotropically. The solvate water molecule was refined anisotropically with occupation factor fixed to 0.50. Further experimental crystallographic details for **4**: $2\theta_{\max} = 144.1^\circ$; reflections collected/unique/used, 27919/7418 [$R_{\text{int}} = 0.0662$]/7418; 634 parameters refined; $(\Delta/\sigma)_{\max} = 0.005$; $(\Delta\rho)_{\max}/(\Delta\rho)_{\min} = 0.418/-0.705 \text{ e}/\text{\AA}^3$; R/R_w (for all data), 0.0814/0.1110. Hydrogen atoms were located by difference maps and were refined isotropically, except those of the methyl groups which were introduced at calculated positions as riding on bonded atoms. All non-H atoms were refined anisotropically. The crystals of **5** showed poor diffraction ability (despite their sufficient size) and signs of twinning. Data were collected to $2\theta_{\max} = 54^\circ$ but only those to $2\theta_{\max} = 45^\circ$ were used for the refinement, since in greater θ values more than 50% of the collected data were unobserved. The twinning problem was handled by omitting reflections showing large F^2_o compared to the expected F^2_c values because an exact twin law could not be found. As it was proved after the solution of the structure, compound **5** is analogous to **4** thus we felt that the complete structural characterization would not add further significant information to our work. Therefore, we have not attempted to improve the quality of the crystals. Further experimental crystallographic details for **5**: $2\theta_{\max} = 45^\circ$; reflections collected/unique/used, 40444/5493 [$R_{\text{int}} = 0.1240$]/5493; 554 parameters refined; $(\Delta/\sigma)_{\max} = 0.017$; $(\Delta\rho)_{\max}/(\Delta\rho)_{\min} = 2.162/-0.608 \text{ e}/\text{\AA}^3$; R/R_w (for all data), 0.1204/0.2448. Hydrogen atoms

were introduced at calculated positions as riding on bonded atoms. All non-H atoms were refined anisotropically.

3. Results and discussion

3.1. Syntheses

Previous investigation of the use of H_2salox in manganese carboxylate chemistry by Perlepes and his co-workers has led to the hexanuclear compounds $[\text{Mn}_6^{\text{III}}(\mu_3\text{-O})_2(\text{O}_2\text{CR})_2(\text{salox})_6(\text{EtOH})_4]$ ($\text{R} = \text{Me}, \text{Ph}$) [14] isolated from the 1:1 $\text{Mn}(\text{O}_2\text{CR})_2 \cdot 2\text{H}_2\text{O}/\text{H}_2\text{salox}$ molar ratio reaction in EtOH. Both complexes exhibit single-molecule magnetism (SMM) behaviour [24], and have been isolated under identical reaction conditions suggesting that the nature of the carboxylate ligand does not affect the identity of the products. Recently Brechin and co-workers have expanded this family of clusters by changing the carboxylate groups and/or by introducing steric bulk at the oximate carbon atom [25]; these modifications led to dramatic improvement of the SMM properties [25b,c]. In order to further investigate the parameter space of this reaction system, we have decided to modify other key factors and in particular: (i) the $\text{Mn}/\text{H}_2\text{salox}$ stoichiometry, (ii) the reaction media, (iii) the source of the manganese ions, (iv) the addition of base and/or counterions, and (v) the crystallization method, in order to study their influence on the metal ions' topology, oxidation state and nuclearity. Thus, reaction of one equivalent of $[\text{Mn}_2^{\text{II}}\text{Mn}^{\text{III}}(\mu_3\text{-O})(\text{O}_2\text{CPh})_6(\text{py})_2(\text{H}_2\text{O})]$ with one equivalent of H_2salox in MeCN and slow evaporation of the reaction mixture afforded green-brown prismatic crystals of $[\text{Mn}_6^{\text{III}}(\mu_3\text{-O})_2(\text{O}_2\text{CPh})_2(\text{salox})_6(\text{py})_2(\text{H}_2\text{O})_2]$ (**1**) and orange cubic crystals of the known mixed-valence hexanuclear complex $[\text{Mn}_4^{\text{II}}\text{Mn}_2^{\text{III}}(\mu_4\text{-O})_2(\text{O}_2\text{CPh})_{10}(\text{py})_2(\text{H}_2\text{O})(\text{MeCN})]$ [20] in mixture. With the identity of **1** established by X-ray crystallography the stoichiometric $\text{Mn}:\text{H}_2\text{salox}$ reaction has been performed which afforded pure **1** for further physical measurements (Scheme 1). Further investigation of



Scheme 1. The synthetic routes employed for the preparation of **1–5** (see text for details).

the reaction media, by reaction of one equivalent of $[\text{Mn}_2^{\text{III}}\text{Mn}^{\text{II}}(\mu_3\text{-O})(\text{O}_2\text{CPh})_6(\text{py})_2(\text{H}_2\text{O})]$ with three equivalents of H_2salox in Me_2CO afforded compound $[\text{Mn}_6^{\text{III}}\text{O}_2(\text{O}_2\text{CPh})_2(\text{salox})_6(\text{Me}_2\text{CO})_2(\text{H}_2\text{O})_2]$ (**2**) either by slow evaporation or layering of Et_2O or vapour diffusion of Et_2O or $\text{Et}_2\text{O}/n\text{-hexane}$ (Scheme 1).

Compounds **1** and **2** are quite similar to the previously reported hexanuclear complexes $[\text{Mn}_6(\mu_3\text{-O})_2(\text{O}_2\text{CR})_2(\text{salox})_6(\text{EtOH})_4]$ ($\text{R} = \text{Me}, \text{Ph}$), suggesting that these species are spontaneously formed, perhaps due to their thermal and/or thermodynamic stability, and/or their insolubility in the reaction solvent. Thus, changes in the source of the manganese ions and the reaction media have not affected the identity of the product isolated, whereas the change of the reactants stoichiometry (excess of manganese ions in the case of **1**) most likely promotes the simultaneous isolation of the known mixed-valence compound $[\text{Mn}_4^{\text{II}}\text{Mn}_2^{\text{III}}(\mu_4\text{-O})_2(\text{O}_2\text{CPh})_{10}(\text{py})_2(\text{H}_2\text{O})(\text{MeCN})]$. Of course the presence of other more soluble species in the reaction mixture cannot be excluded.

In order to examine the influence of the base and/or counterions we have employed reactions analogous to those leading to **1** and **2** in the presence of NaOMe and/or $\text{NaClO}_4 \cdot \text{H}_2\text{O}$. Thus, reaction of one equivalent of $[\text{Mn}_2^{\text{II}}\text{Mn}^{\text{III}}(\mu_3\text{-O})(\text{O}_2\text{CPh})_6(\text{py})_2(\text{H}_2\text{O})]$ with three equivalents of H_2salox in the presence of six equivalents of NaOMe in MeOH yielded compound $[\text{Mn}_6^{\text{III}}\text{O}_2(\text{O}_2\text{CPh})_2(\text{salox})_6(\text{MeOH})_4]$ (**3**), which is completely analogous to **1** and **2**. On the other hand, the analogous reaction in MeCN yielded only the 1D complex $[\text{Mn}_3^{\text{III}}\text{Na}(\mu_3\text{-O})(\text{O}_2\text{CPh})_2(\text{salox})_3(\text{MeCN})]_n$ (**4**) whose structure is completely different than **1–3**, whereas the same reaction mixture in Me_2CO afforded only **2** as confirmed by X-ray crystallography (Scheme 1). Finally the reaction of one equivalent of $(\text{NBu}^t_4)[\text{Mn}_2^{\text{II}}\text{O}_2(\text{O}_2\text{CPh})_9(\text{H}_2\text{O})]$ with four equivalents of H_2salox in the presence of eight equivalents of $\text{NaClO}_4 \cdot \text{H}_2\text{O}$ in MeCN also afforded compound **4**, whereas the analogous reaction in Me_2CO afforded the 1D complex $[\text{Mn}_3^{\text{III}}\text{Na}(\mu_3\text{-O})(\text{O}_2\text{CPh})_2(\text{salox})_3(\text{Me}_2\text{CO})]_n$ (**5**) which is analogous to **4** (Scheme 1).

In conclusion, the reaction media, the use of oligonuclear manganese complexes as starting materials and the crystallization methods have not affected the identity of the hexanuclear complexes **1–3**, whereas analogous modifications on the salicylaldoximate iron(III) carboxylate chemistry revealed that the reaction media is determinative for the identity of the product. Trinuclear $[\text{Fe}_3(\mu_3\text{-O})(\text{O}_2\text{CPh})_5(\text{salox})(\text{L}_1)(\text{L}_2)]$ ($\text{L}_1 = \text{L}_2 = \text{MeOH}$, $\text{L}_1 = \text{EtOH}$ and $\text{L}_2 = \text{H}_2\text{O}$ depending on the reaction solvent) [10] or hexanuclear $[\text{Fe}_6(\mu_3\text{-O})_2(\text{O}_2\text{CPh})_{10}(\text{salox})_2(\text{L}_2)]$ ($\text{L} = \text{H}_2\text{O}, \text{MeCONH}_2$) [8a] complexes have been isolated from alcoholic or MeCN solutions, respectively; the former being transformed to the latter by simple recrystallization from MeCN solutions. Compounds **1–3** and $[\text{Fe}_6(\mu_3\text{-O})_2(\text{O}_2\text{CPh})_{10}(\text{salox})_2(\text{L}_2)]$ contain the same $[\text{M}_6^{\text{III}}(\mu_3\text{-O})_2(\mu_2\text{-OR})_2]^{12+}$ core, although the rest of the ligation pattern is different. On the other hand, the presence of sodium ions in the reaction mixtures in MeCN and Me_2CO , either as NaOMe or $\text{NaClO}_4 \cdot \text{H}_2\text{O}$, revealed dramatic changes to the identity of the products isolated yielding the 1D complexes **4** and **5**.

3.2. Description of structures

Compound **1** crystallizes in the triclinic space group $P\bar{1}$ with one molecule per unit cell. The molecular structure of **1** is given in Fig. 1 and selected bond distances and angles are listed in Table 2. The structure contains the $[\text{Mn}_6(\mu_3\text{-O})_2(\mu_2\text{-OR})_2]^{12+}$ core, whose topology consists of six manganese(III) ions arranged as two centrosymmetrically related off-set stacked $[\text{Mn}_3(\mu_3\text{-O})]^{7+}$ subunits bridged by two oximate oxygen atoms ($\text{O}(12)$ and $\text{O}(12')$). In each $[\text{Mn}_3(\mu_3\text{-O})]^{7+}$ subunit, there are two $\text{Mn} \cdots \text{Mn}$ pairs $[\text{Mn}(1)/\text{Mn}(3)$ and $\text{Mn}(1)/\text{Mn}(2)]$ bridged by a μ_2 oxide and a $\mu_2\text{-}\kappa\text{O}:\kappa\text{O}':\kappa\text{N}$ salox^{2-} ligand, while the third pair $[\text{Mn}(2)/\text{Mn}(3)]$ is further bridged by a μ_2 benzoate ligand. The coordination

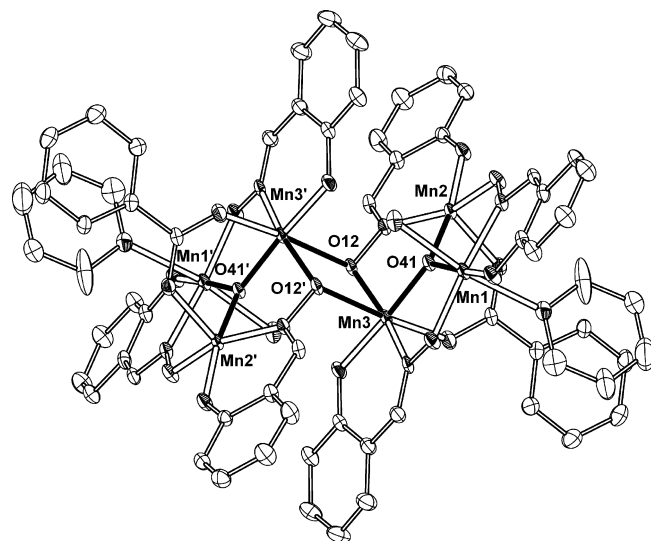


Fig. 1. Partially labelled ORTEP plot of **1** with ellipsoids drawn at the 30% probability level. For clarity hydrogen atoms have been omitted. Primed atoms are generated by symmetry ($' = -x, 2 - y, 1 - z$).

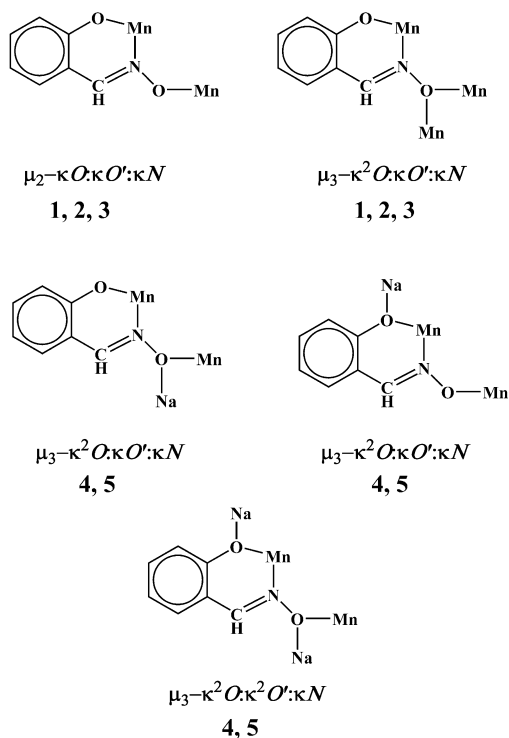
geometry around $\text{Mn}(1)$ is distorted octahedral where the equatorial positions are occupied by one salox^{2-} ligand (through $\text{O}_{\text{phenolic}}$ and $\text{N}_{\text{oximate}}$ atoms), the $\text{O}_{\text{oximate}}$ atom of a second salox^{2-} ligand and the oxide group, while the Jahn–Teller axis of the octahedron is completed by a pyridine and a coordinated water molecule. The coordination geometry around $\text{Mn}(2)$ is square pyramidal comprised by one salox^{2-} ligand (through $\text{O}_{\text{phenolic}}$ and $\text{N}_{\text{oximate}}$ atoms), the $\text{O}_{\text{oximate}}$ atom of a second salox^{2-} ligand and the oxide group occupying the equatorial plane, while the apical position is occupied by an oxygen atom of the μ_2 benzoate ligand. Finally, the coordination geometry about $\text{Mn}(3)$ is distorted octahedral comprised by one salox^{2-} ligand (through $\text{O}_{\text{phenolic}}$ and $\text{N}_{\text{oximate}}$ atoms), the oxide group and the $\text{O}_{\text{oximate}}$ atom of a second salox^{2-} directed in the equatorial plane of the octahedron, while the Jahn–Teller positions are completed by a benzoate oxygen and an $\text{O}_{\text{oximate}}$ atom of a third salox^{2-} ligand. Thus, in each $[\text{Mn}_3(\mu_3\text{-O})]$ subunit two of the salox^{2-} ligands adopt the common $\mu_2\text{-}\kappa\text{O}:\kappa\text{O}':\kappa\text{N}$ coordination mode, while the third one presents the rare $\mu_3\text{-}\kappa^2\text{O}:\kappa\text{O}':\kappa\text{N}$ coordination mode (Scheme 2), that has been also observed in $[\text{Mn}_6(\mu_3\text{-O})_2(\text{O}_2\text{CR})_2(\text{salox})_6(\text{R}'\text{OH})_4]$ [14,25a], $[\text{Fe}_6(\mu_3\text{-O})_2(\text{O}_2\text{CPh})_{10}(\text{salox})_2(\text{H}_2\text{O})_2]$ [8a], and in $[\text{M}_6^{\text{III}}(\mu_3\text{-O})_2(\text{salox})_6(\mu_2\text{-O}_2\text{CR})_2(\text{OH}_2)_2(\text{RCN})_2]$ ($\text{M} = \text{V}^{\text{III}}, \text{Cr}^{\text{III}}, \text{Mn}^{\text{III}}, \text{Fe}^{\text{III}}, \text{RCO}_2^- = \text{Ph}_3\text{CCO}_2^-, \text{Me}_3\text{CCO}_2^-, \text{Ph}_2\text{C}(\text{OH})\text{CO}_2^-, \text{PhCO}_2^-, \text{C}_2\text{H}_5\text{CO}_2^-$) [26], but also in trinuclear and tetranuclear complexes [27].

The three Mn^{III} ions in each $[\text{Mn}_3(\mu_3\text{-O})]^{7+}$ subunit form an almost isosceles triangle (see Table 2). The $\text{Mn}(2) \cdots \text{Mn}(3)$ separation (3.158(2) Å) is shorter than the other two in the triangular subunit (3.248(5), 3.273(5) Å) due to the presence of the extra benzoate bridge. The $\text{Mn} \cdots \text{Mn}$ distance in the central $[\text{Mn}_2(\mu_2\text{-O})_2]$ core is 3.335(5). The central $\mu_3\text{-O}^{2-}$ ion in each $[\text{Mn}_3(\mu_3\text{-O})]$ subunit is displaced at 0.17 Å out of the $[\text{Mn}_3]$ mean plane, an observation that has been also seen in the analogous compound $[\text{Mn}_6(\mu_3\text{-O})_2(\text{O}_2\text{CR})_2(\text{salox})_6(\text{R}'\text{OH})_4]$ [14,25a] as well as in the trinuclear complexes $[\text{Mn}_3(\mu_3\text{-O})(\text{O}_2\text{CR})_3(\text{mpko})_3](\text{ClO}_4)$ ($\text{R} = \text{Me}, \text{Et}, \text{Ph}$; $\text{mpkoH} = \text{methyl-2-pyridyl ketone oxime}$, 0.30 Å) [28]. The $\text{Mn}-\text{O}_{\text{oxo}}$ bond distances are in the range 1.863–1.881 Å. The $\text{Mn}-\text{O}_{\text{phenoxo}}$ and the $\text{Mn}-\text{N}_{\text{oximate}}$ bond lengths are ~ 1.86 and ~ 2.0 Å, respectively. The $\text{Mn}-\text{O}_{\text{oximate}}$ chelating bond distances are ~ 1.94 Å while the corresponding bridging bond distances are significantly longer (2.420 Å). All the salox^{2-} ligands are planar and make an angle of 5.1°, 13.3° and 28.7° (for the salox^{2-} ligands defined by $\text{O}(1)$, $\text{O}(11)$, and $\text{O}(21)$, respectively) with the $[\text{Mn}_3]$ mean

Table 2
Selected bond distances (Å) and angles (°) for complex **1** · 6MeCN

Distances					
Mn(1)–O(1)	1.859(3)	Mn(2)–O(11)	1.864(3)	Mn(3)–O(21)	1.866(3)
Mn(1)–O(41)	1.882(3)	Mn(2)–O(41)	1.862(3)	Mn(3)–O(41)	1.868(3)
Mn(1)–O(22)	1.922(3)	Mn(2)–O(2)	1.900(3)	Mn(3)–O(12)	1.942(3)
Mn(1)–N(1)	1.998(4)	Mn(2)–N(11)	2.011(4)	Mn(3)–N(21)	1.998(4)
Mn(1)–O(w)	2.310(4)	Mn(2)–O(31)	2.123(4)	Mn(3)–O(32)	2.137(4)
Mn(1)–N(41)	2.391(4)	Mn(1)···Mn(2)	3.273(5)	Mn(3)–O(12')	2.419(3)
Mn(1)···Mn(3)	3.248(5)	Mn(2)···Mn(3)	3.158(2)	Mn(3)···Mn(3')	3.335(5)
Angles					
O(1)–Mn(1)–O(41)	174.5(2)	O(11)–Mn(2)–O(41)	169.4(2)	O(21)–Mn(3)–O(41)	175.6(2)
O(1)–Mn(1)–O(22)	88.8(2)	O(11)–Mn(2)–O(2)	87.2(1)	O(21)–Mn(3)–O(12)	88.4(1)
O(41)–Mn(1)–O(22)	92.3(1)	O(41)–Mn(2)–O(2)	91.0(2)	O(41)–Mn(3)–O(12)	89.8(1)
O(1)–Mn(1)–N(1)	91.9(2)	O(11)–Mn(2)–N(11)	89.0(2)	O(21)–Mn(3)–N(21)	90.9(2)
O(41)–Mn(1)–N(1)	87.6(1)	O(41)–Mn(2)–N(11)	89.4(1)	O(41)–Mn(3)–N(21)	89.9(1)
O(22)–Mn(1)–N(1)	174.8(2)	O(2)–Mn(2)–N(11)	161.4(2)	O(12)–Mn(3)–N(21)	165.9(2)
O(1)–Mn(1)–O(w)	88.2(2)	O(11)–Mn(2)–O(31)	98.1(2)	O(21)–Mn(3)–O(32)	94.1(2)
O(41)–Mn(1)–O(w)	86.3(1)	O(41)–Mn(2)–O(31)	92.5(1)	O(41)–Mn(3)–O(32)	90.1(1)
O(22)–Mn(1)–O(w)	97.8(2)	O(2)–Mn(2)–O(31)	104.2(2)	O(12)–Mn(3)–O(32)	96.6(2)
N(1)–Mn(1)–O(w)	87.5(2)	N(11)–Mn(2)–O(31)	94.3(2)	N(21)–Mn(3)–O(32)	97.5(2)
O(1)–Mn(1)–N(41)	89.3(2)	Mn(1)–O(41)–Mn(2)	121.9(2)	O(21)–Mn(3)–O(12')	88.9(1)
O(41)–Mn(1)–N(41)	96.1(1)	Mn(1)–O(41)–Mn(3)	120.1(2)	O(41)–Mn(3)–O(12')	86.8(1)
O(22)–Mn(1)–N(41)	90.9(2)	Mn(2)–O(41)–Mn(3)	115.7(2)	O(12)–Mn(3)–O(12')	80.8(1)
N(1)–Mn(1)–N(41)	83.9(2)	Mn(3)–O(12)–Mn(3')	99.2(1)	O(32)–Mn(3)–O(12')	176.0(1)
Ow–Mn(1)–N(41)	170.9(2)			N(21)–Mn(3)–O(12')	85.1(1)

Symmetry transformations used to generate equivalent atoms: ' = -x, 2 - y, 1 - z.



Scheme 2. The coordination modes of salox^{2-} ligands in the structures of **1**–**5** (see text for details).

plane. The benzoate ligands are coordinated through the common *syn,syn* $\mu_2\text{-}\kappa\text{O}:\kappa\text{O}'$ mode. The Mn–O_{carboxylate} bond distances are ~2.13 Å. There is a moderate twisting of the Mn–O–N–Mn moieties within each Mn₃ subunit; this is evidenced by the Mn–N–O–Mn torsion angles which are 5.9°, 22.3° and 19.8° for the Mn(1)/Mn(2), Mn(2)/Mn(3) and Mn(3)/Mn(1) pairs (and their symmetry-equivalents), respectively.

Compound **2** crystallizes in the tetragonal space group $I4_1/a$, with eight molecules per unit cell, and compound **3** crystallizes in the triclinic space group $P\bar{1}$ with two half molecules in the asym-

metric unit. The molecular structures of **2** and **3** (Figs. 2 and 3, respectively) are completely analogous to **1** and they will not be discussed further. Selected bond distances and angles are given as **Supplementary material** (Tables S1 and S2, respectively); a comparison of their structural characteristics with those of **1** is given in **Table 4**.

Compound **4** crystallizes in the monoclinic space group $P2_1/c$ with one molecule per asymmetric unit. The molecular structure of **4** consists of anionic trinuclear oxo-centered units, $[\text{Mn}_3^{\text{III}}(\mu_3\text{-O})(\text{O}_2\text{CPh})_2(\text{salox})_3]^-$, sodium cations and MeCN molecules. An ORTEP plot of the structure of **4** is given in **Fig. 4**, selected bond distances and angles are listed in **Table 3**. The trinuclear anion contains a central $[\text{Mn}_3(\mu_3\text{-O})]^{7+}$ core, in which two Mn···Mn pairs [Mn(1)/Mn(2) and Mn(2)/Mn(3)] are bridged by a μ_2 oxide and a $\mu_2\text{-}\kappa\text{O}:\kappa\text{O}':\kappa\text{N}$ salox^{2-} ligand, while the third pair [Mn(1)/Mn(3)] is further bridged by a μ_2 benzoate ligand. The coordination geometry

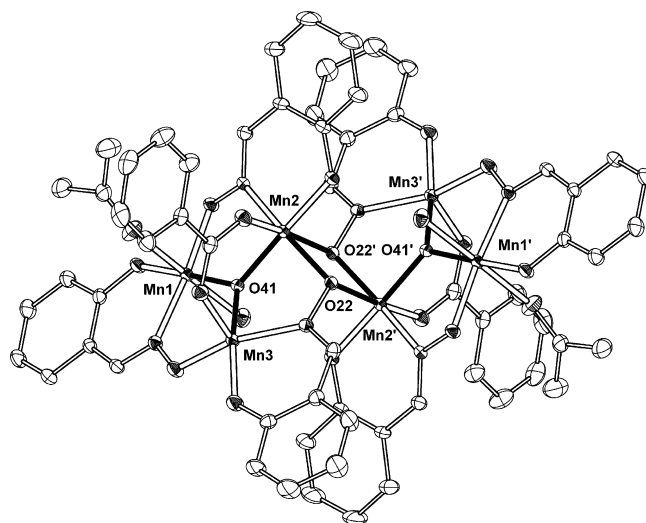
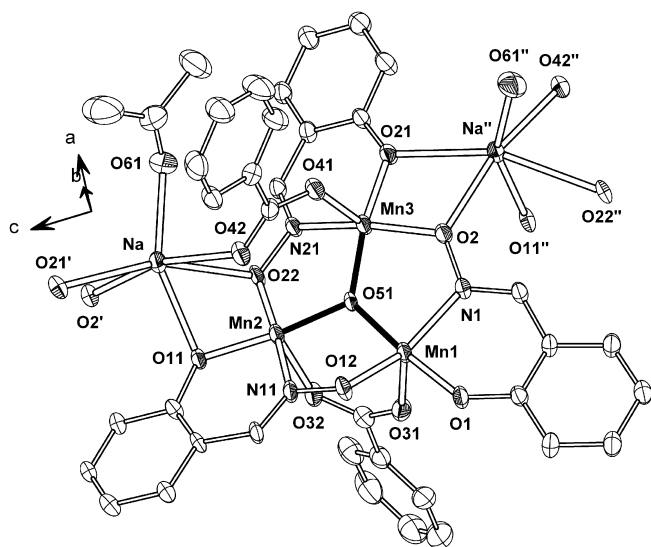


Fig. 2. Partially labelled ORTEP plot of **2** with ellipsoids drawn at the 30% probability level. For clarity hydrogen atoms have been omitted. Primed atoms are generated by symmetry (' = 1 - x, 1 - y, -z).

Table 3
Selected bond distances (Å) and angles (°) for complex **4** · nMeCN

Distances					
Mn(1)–O(1)	1.865(3)	Mn(2)–O(51)	1.845(2)	Mn(3)–O(21)	1.856(3)
Mn(1)–O(51)	1.867(2)	Mn(2)–O(11)	1.869(3)	Mn(3)–O(51)	1.865(2)
Mn(1)–O(12)	1.915(3)	Mn(2)–O(22)	1.920(2)	Mn(3)–O(2)	1.906(3)
Mn(1)–N(1)	1.992(3)	Mn(2)–N(11)	2.028(3)	Mn(3)–N(21)	2.003(3)
Mn(1)–O(31)	2.170(3)	Mn(2)–O(41)	2.045(3)	Mn(3)–O(32)	2.085(3)
Na–O(22')	2.406(3)	Na–N(31)	2.419(5)	Na–O(42)	2.490(3)
Na–O(1)	2.414(3)	Na–O(11')	2.451(3)	Na–O(12)	2.673(3)
Mn(1)···Mn(2)	3.206(1)	Mn(1)···Mn(3)	3.138(1)	Mn(2)···Mn(3)	3.305(1)
Mn(1)···Na	3.187(2)	Mn(2)···Na''	3.443(2)		
Angles					
O(1)–Mn(1)–O(51)	169.4(1)	O(51)–Mn(2)–O(11)	167.5(1)	O(21)–Mn(3)–O(51)	174.8(1)
O(1)–Mn(1)–O(12)	86.9(1)	O(51)–Mn(2)–O(22)	89.2(1)	O(21)–Mn(3)–O(2)	90.7(1)
O(51)–Mn(1)–O(12)	92.7(1)	O(11)–Mn(2)–O(22)	85.7(1)	O(51)–Mn(3)–O(2)	90.9(1)
O(1)–Mn(1)–N(1)	90.8(1)	O(51)–Mn(2)–N(11)	89.2(1)	O(21)–Mn(3)–N(21)	90.7(1)
O(51)–Mn(1)–N(1)	89.0(1)	O(11)–Mn(2)–N(11)	90.7(1)	O(51)–Mn(3)–N(21)	85.8(1)
O(12)–Mn(1)–N(1)	176.2(1)	O(22)–Mn(2)–N(11)	155.2(1)	O(2)–Mn(3)–N(21)	155.1(1)
O(1)–Mn(1)–O(31)	98.6(1)	O(51)–Mn(2)–O(41)	95.9(1)	O(21)–Mn(3)–O(32)	91.3(1)
O(51)–Mn(1)–O(31)	92.1(1)	O(11)–Mn(2)–O(41)	96.7(1)	O(51)–Mn(3)–O(32)	93.4(1)
O(12)–Mn(1)–O(31)	93.4(1)	O(22)–Mn(2)–O(41)	111.0(0)	O(2)–Mn(3)–O(32)	98.1(1)
N(1)–Mn(1)–O(31)	89.9(1)	N(11)–Mn(2)–O(41)	93.9(1)	N(21)–Mn(3)–O(32)	106.8(1)
O(22')–Na–O(1)	86.3(1)	N(31)–Na–O(11')	108.9(1)	O(22')–Na–O(12)	99.2(1)
O(22')–Na–N(31)	108.0(1)	O(22')–Na–O(42)	165.2(1)	O(1)–Na–O(12)	61.2(1)
O(1)–Na–N(31)	149.0(1)	O(1)–Na–O(42)	79.1(1)	N(31)–Na–O(12)	88.8(1)
O(22')–Na–O(11')	64.1(1)	N(31)–Na–O(42)	83.8(1)	O(11')–Na–O(12)	158.3(1)
O(1)–Na–O(11')	102.1(1)	O(11')–Na–O(42)	121.5(1)	O(42)–Na–O(12)	71.4(1)
Mn(2)–O(51)–Mn(3)	125.9(1)	Mn(2)–O(51)–Mn(1)	119.5(1)	Mn(3)–O(51)–Mn(1)	114.5(1)
Mn(1)–O(12)–Na	86.3(1)	Mn(1)–O(1)–Na	95.4(1)	Mn(2)–O(11)–Na''	104.9(1)
Mn(2)–O(22)–Na''	104.9(1)				

Symmetry transformations used to generate equivalent atoms: ' = x, 0.5 – y, –0.5 + z; '' = x, 0.5 – y, 0.5 + z.

**Fig. 5.** Partially labelled ORTEP plot of a small fragment of the chains of **5** with ellipsoids drawn at the 30% probability level. For clarity hydrogen atoms have been omitted. Symmetry transformations used to generate equivalent atoms: ' = x, 0.5 – y, 0.5 + z; '' = x, 0.5 – y, –0.5 + z.

7.63 cm³ mol^{–1} K at 30 K, and then increases to a maximum of 9.22 cm³ mol^{–1} K at 10 K, before falling to 4.71 cm³ mol^{–1} K at 2 K. This overall behaviour shows the interplay of both ferro- and antiferromagnetic interactions. The drop below 10 K is associated with zero-field splitting effects of the Mn^{III} ions. The maximum around 10 K is field-dependent, being suppressed and shifted to higher temperatures with increase of the applied magnetic field. This is attributed to the additional Zeeman splitting of the ground multiplet.

The overall behavior is very similar to that encountered in complexes [Mn₆(μ₃-O)₂(O₂CR)₂(salox)₆(EtOH)₄] (R = Me, Ph) [8], which is in accord with the structural similarities of the complexes. *M* versus *HT*^{–1} plots (Fig. 6) confirm that in **1** an *S* = 4 ground state is also stabilized. Fits of the low-temperature data, and assuming a well-isolated ground state, yield values of *|D|* ~ 0.5 cm^{–1} and *g* = 2.00 for the ground state. The magnitude of *D* for the ground state of complex **1**, is lower than the values previously reported (*|D|* = 1.22 [14] and 1.39 cm^{–1} [25a]) for the respective Mn₆ complexes with *S* = 4 ground states. Although these fits qualitatively confirm the ground state as an *S* = 4 one, they fail to accurately reproduce the data, probably due to the existence of low-lying excited states. This is to be expected, given the relatively weak exchange couplings between Mn^{III} ions, which lead to a closely

Table 4
Structural characteristics of compounds **1–5**

	Mn···Mn in [Mn ₃ O] core (Å)	Mn···Mn in [Mn ₂ O ₂] core (Å)	Displacement of O ^{2–} /[Mn ₃] plane (Å)	Mn–N–O–Mn torsion angle (average) (°)
1	3.159(2)–3.274(5)	3.335(5)	0.17	6.1, 19.7, 22.5 (16.1)
2	3.163(2)–3.268(2)	3.314(2)	0.17	1.1, 21.6, 24.5 (15.7)
3 ^a	3.150(1)–3.278(2)	3.287(2)	0.18	6.6, 22.7, 32.9 (20.7)
	3.164(2)–3.262(2)	3.304(2)	0.20	13.1, 13.3, 29.8 (18.7)
4	3.138(1)–3.305(1)		0.00	0.8, 16.7, 22.1 (13.2)
5	3.142(2)–3.301(2)		0.00	2.5, 14.0, 22.6 (13.0)

^a For the two crystallographically independent molecules in the asymmetric unit.

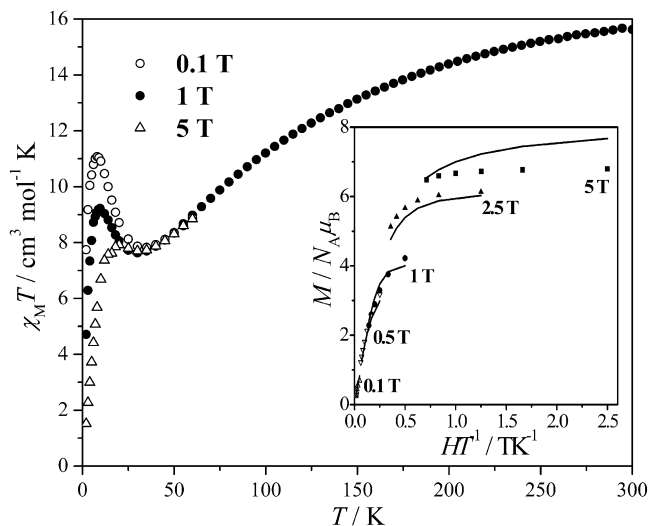


Fig. 6. $\chi_M T$ vs. T data for **1** under various magnetic fields. The M vs. HT^{-1} dependence along with a fit assuming an isolated $S = 4$ ground state are shown in the inset.

spaced energy spectrum. Thus, the values of the above fits should not be considered as quantitatively accurate.

The $S = 4$ ground state is in accord [25] with the moderate twisting of the Mn–N–O–Mn moieties within each Mn_3 subunit, the average torsion angle being $\alpha_v = 16^\circ$. Brechin and co-workers recently showed [25b,c] that when this twisting in this family of Mn_6^{III} SMMs becomes severe (as a consequence of the use of bulky substituents on the oximate carbon), e.g. $\alpha_v = 36.5^\circ$ or 39.1° , the resulting ground state is $S = 12$ and record U_{eff} values up to 86.4 K can be achieved.

The $\chi_M T$ product of **5** (Fig. 7) at 300 K (0.5 T) is $6.64 \text{ cm}^3 \text{ mol}^{-1} \text{ K}$, lower than the theoretically expected value for three non-interacting $S = 2$ spins ($9.00 \text{ cm}^3 \text{ mol}^{-1} \text{ K}$, $g = 2$), indicating the interplay of antiferromagnetic interactions. Upon cooling, this rapidly decreases, attaining a value of $0.51 \text{ cm}^3 \text{ mol}^{-1} \text{ K}$ at 2 K.

In order to interpret the experimental data, an isosceles model of three interacting $S = 2$ spins was assumed, based on the repeating unit of the complex. Due to its polymeric structure, intra-unit interactions are expected, while significant single-ion zero-field splitting parameters D , are also common for Mn^{III} complexes. The

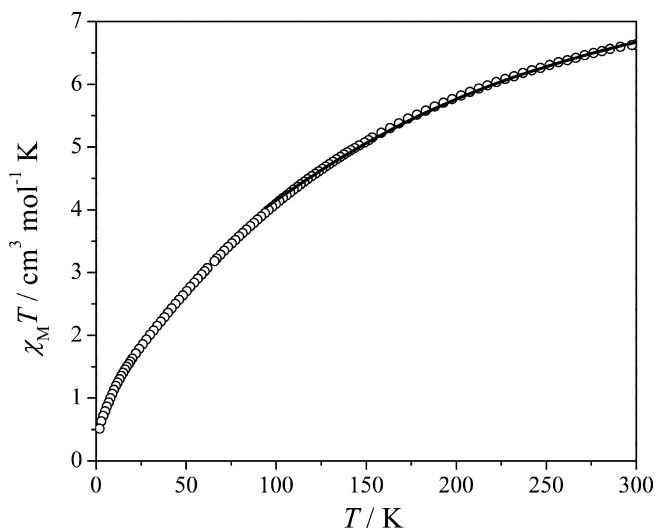


Fig. 7. $\chi_M T$ vs. T data for **5** and best fit according to the model described in the text.

former was accounted for by a mean-field correction term zj , while the latter by an axial zfs parameter D , common for all spins ($D = D_1 = D_2 = D_3$). Initial fitting attempts over 2–300 K yielded very poor results. It was then decided that the intramolecular interactions might be too complex to be successfully accounted for by a mean-field term, while the single-ion zfs parameters might be substantially different for the three sites. In addition, it was also acknowledged that since both parameters zj and D are mainly manifested in the low temperature range, inclusion of both in our model might lead to overparametrization of our problem. Thus, a simpler model was used, considering only the intra-unit exchange couplings, while the data over the 300–100 K range were fitted. The corresponding Hamiltonian is given in Eq. (1):

$$\hat{H} = -2[J_1(\hat{S}_1\hat{S}_2 + \hat{S}_1\hat{S}_3) + J_2\hat{S}_2\hat{S}_3] \quad (1)$$

Best-fit parameters for this model were $J_1 \sim J_2 = -11.8 \text{ cm}^{-1}$, $g = 2.01$ with $R = 4.1 \times 10^{-5}$, corresponding to a $S = 2$ ground state.

3.3.2. AC susceptibility

Given the pronounced similarities of **1** with $[Mn_6(\mu_3-O)_2(O_2CR)_2(salox)_6(EtOH)_4]$ ($R = \text{Me, Ph}$), we decided to test whether it also behaves as an SMM. Thus, in order to probe its relaxation properties, AC susceptibility experiments were carried out at low temperatures (Fig. 8). These showed characteristic out-of-phase signals attributed to slow magnetic relaxation phenomena. The signals show clear maxima between 2.13 K (10 Hz) and 3.50 K (1400 Hz). For lower frequencies the maxima occur below 1.9 K, which is the lower limit of our instrument. Fits of these data to an Arrhenius law, $\tau = \tau_0 \cdot e^{U_{eff}/k_B T}$, yielded parameters

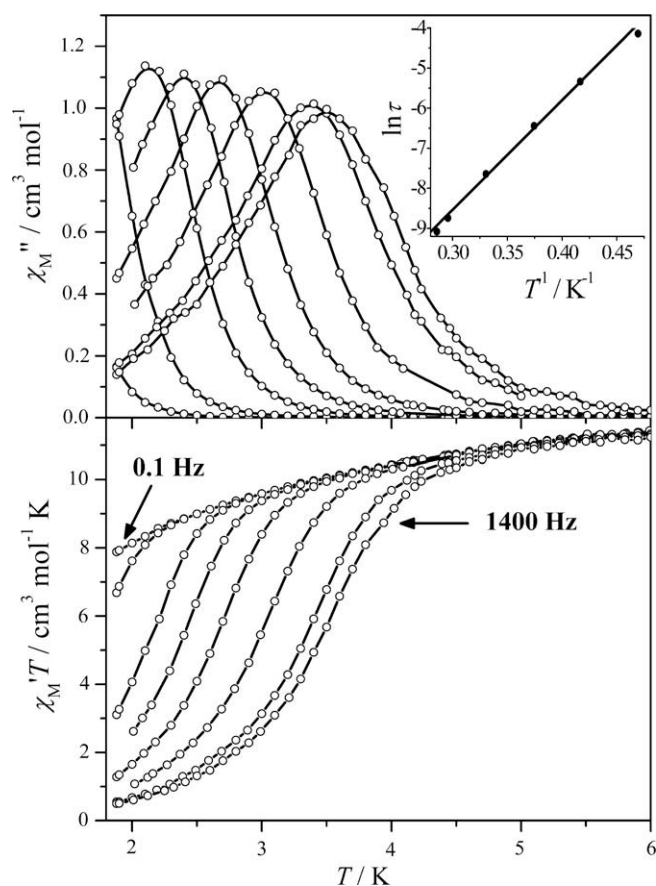


Fig. 8. $\chi'_M T$ (top) and $\chi''_M T$ vs. T data for **1** between 1.9 and 6 K for oscillating magnetic fields of 0.1, 1, 10, 33, 100, 333, 1000 and 1400 Hz. A fit of the out-of-phase data to an Arrhenius law is shown in the inset.

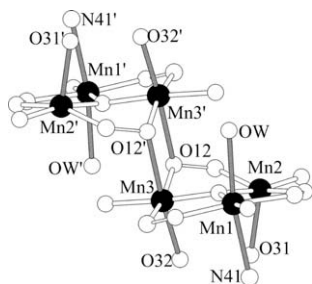


Fig. 9. Simplified view of **1**, showing the coordination spheres of the Mn^{III} ions. The Jahn-Teller elongated bonds (shown in gray) are roughly parallel to each other.

$\tau_0 = 5.5 \times 10^{-8}$ s and $U_{\text{eff}} = 27.4$ K = 19.0 cm⁻¹. For an $S = 4$ ground state and considering that $\Delta E = S^2|D| > U_{\text{eff}}$, it turns that the lowest limit for $|D|$ is 1.2 cm⁻¹, or in other words $D < -1.2$ cm⁻¹. These results are in close agreement with the results obtained for $[\text{Mn}_6(\mu_3\text{-O})_2(\text{O}_2\text{CR})_2(\text{salox})_6(\text{R}'\text{OH})_4]$ (R = H, Me, Ph; R' = Me, Et) [14,25a].

The relatively high value of D predicted by the relaxation experiments deserves some comment. Generally speaking, the anisotropy of the ground state is related to the single-ion anisotropies of the coupled spins. The projection of each single-ion anisotropy on the molecular anisotropy axis (i.e. the z -axis) contributes to the total anisotropy. High-spin ($S = 2$) Mn^{III} ions, are highly anisotropic ions, with their easy axes coinciding with their Jahn-Teller axes. In the case of **1** we observe that the Jahn-Teller elongation axes are roughly parallel (Fig. 9). This should have an important effect on the total D value. We should note that for a D value of -1.2 cm⁻¹, a cluster like Mn₁₂ ($S = 10$) should present a spin-reversal energy barrier of ca. 120 cm⁻¹. This relatively high D value should be responsible for the fact that clear out-of-phase signals are observed despite the relatively low spin ($S = 4$) of the ground state.

3.4. Solid state NMR studies

Nuclear magnetic resonance is a powerful tool in order to probe the internal fields that are present in paramagnetic and magnetic solids. In particular the nuclear T_1 spin-lattice relaxation is sensitive to the electron spin dynamics of the system since the nuclei under investigation probe the fluctuating local magnetic fields induced at the nuclear sites through the hyperfine interaction.

The ¹H T_1 spin-lattice relaxation time of complex **1** was measured at an applied magnetic field $H = 2.4$ T, between room and liquid-helium temperatures. The nuclear relaxation rate $1/T_1$ as a function of temperature is shown in Fig. 10.

At high temperatures $1/T_1$ is nearly temperature independent while below 70 K the rate increases exponentially with an appearance of a peak at around 15 K. This behaviour has been frequently encountered in previous ¹H NMR studies of molecular clusters, rings and single-molecule magnets and it is observed when the temperature is of the order of the magnetic exchange constant J/k_B between the magnetic ions [33].

In these molecular clusters, due to finite size of the spin system, the low-lying energy states are well separated among themselves and at low temperatures, the spin dynamics is governed by magnetic excitations between the ground state and the next excited state separated by an energy difference Δ . This energy difference Δ is largely determined by the exchange interaction J/k_B and the peak of the nuclear relaxation rate $1/T_1$ occurs when the temperature is of the order of the energy gap. Thus the appearance of the NMR peak provide us with a direct estimate of the energy difference between the ground state and the first excited state and can be compared with results of magnetic measurements.

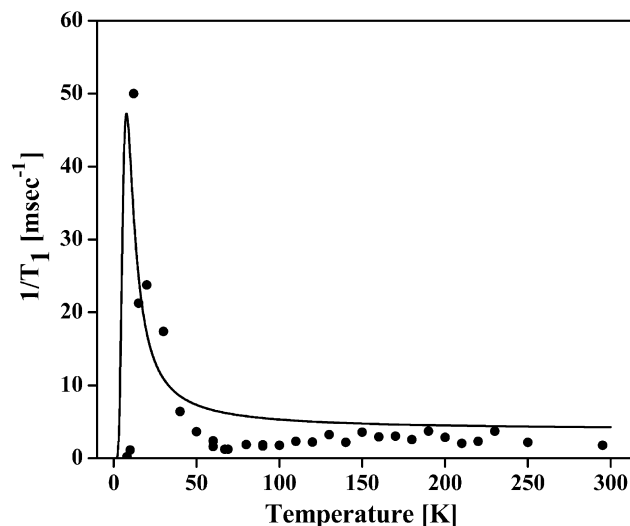


Fig. 10. ¹H NMR $1/T_1$ spin-lattice relaxation rate of complex **1** as a function of temperature (solid line represents the fitted data according to Eq. (2)).

For the analysis of the NMR data, we adopt a simple model, originally proposed by Hardeman et al. [34] based on a two level scheme for the fluctuations of the orientation of the magnetic moment.

In this model the NMR relaxation is caused by the local field fluctuations originating from the magnetic excitations from the ground state to the excited state, separated by the energy difference Δ . Assuming that the Mn spin system remains in the ground state for an average time τ_0 and in the excited state for a lifetime τ_1 , during which an effective transverse local field h_{\perp} appears at the nuclear site, the relaxation rate is expressed as [34]

$$\frac{1}{T_1} = (\gamma_N h_{\perp})^2 \frac{\tau_1 \tau_0}{(\tau_1 + \tau_0)^2} \frac{\tau}{(\omega_N \tau)^2 + 1} \quad (2)$$

where

$$\frac{1}{\tau} = \frac{1}{\tau_0} + \frac{1}{\tau_1},$$

γ_N is the proton gyromagnetic ratio and ω_N is the Larmor angular frequency.

This model has been frequently employed for the nuclear magnetic relaxation in paramagnets [29d,33a,35].

Considering an activation-type process for the excitation, we set

$$\frac{1}{\tau_0} = B_0 \exp\left(-\frac{\Delta}{k_B T}\right) \quad (3)$$

where Δ represents the energy-level spacing between the ground state and the first excited state. For the lifetime τ_1 we consider a temperature independent term:

$$1/\tau_1 = C_1 \quad (4)$$

Setting $\nu_N = 100$ MHz ($H = 4.7$ T), and using Eqs. (3) and (4), the experimental NMR points are fitted to Eq. (2), shown as solid line in Fig. 10. The fitted parameters are $\Delta/k_B = 20$ K for the energy gap and $B_0 = 5 \times 10^9$ s⁻¹ and $C = 5 \times 10^8$ s⁻¹, which are slow fluctuations of the order of the Larmor frequency. We observe that the line describes the overall experimental features rather well.

Therefore the NMR analysis of the low-frequency dynamics of the Mn electron spin system clearly demonstrates the existence of a sizeable energy gap between the ground state and the first excited multiple. Also we have given a measure of the magnitude

of the local-field fluctuations present in the electronic spin system.

4. Conclusions

Three hexanuclear compounds presenting the $[\text{Mn}_6(\mu_3\text{-O})_2(\mu_2\text{-OR})_2]^{12+}$ core, complexes $[\text{Mn}_6^{\text{III}}(\mu_3\text{-O})_2(\text{O}_2\text{CPh})_2(\text{salox})_6(\text{L}_1)_2(\text{L}_2)_2]$ ($\text{L}_1 = \text{py}$, $\text{L}_2 = \text{H}_2\text{O}$ (**1**); $\text{L}_1 = \text{Me}_2\text{CO}$, $\text{L}_2 = \text{H}_2\text{O}$ (**2**); $\text{L}_1 = \text{L}_2 = \text{MeOH}$ (**3**)) have been prepared. The influence of the reactants stoichiometry, the reaction media, the use of oligonuclear manganese clusters as starting materials and crystallization, on the isolation of the congener compounds **1–3** is negligible. On the other hand, the presence of Na^+ ions (either as NaOMe or $\text{NaClO}_4 \cdot \text{H}_2\text{O}$) in the corresponding MeCN and Me_2CO solutions, dramatically influenced the identity of the products, yielding the 1D complexes $[\text{Mn}_3^{\text{III}}\text{Na}(\mu_3\text{-O})(\text{O}_2\text{CPh})_2(\text{salox})_3(\text{S})]_n$ ($\text{S} = \text{MeCN}$ (**4**), Me_2CO (**5**)). The magnetic properties of the representative compounds **1** (hexanuclear) and **5** (polymeric) have been studied. The magnetic susceptibility measurements from polycrystalline samples of **1** revealed the interplay of both ferro- and antiferromagnetic interactions stabilizing an $S = 4$ ground state as confirmed by M versus HT^{-1} plots. The AC susceptibility measurements at 1.9–6 K showed characteristic out-of-phase signals due to slow magnetic relaxation phenomena. Fits of the AC data to the Arrhenius law, yielded parameters $\tau_0 = 5.5 \times 10^{-8}$ s and $U_{\text{eff}} = 27.4$ K = 19.0 cm $^{-1}$. The magnetic behavior of **1** is analogous to the SMM behavior displayed by the prototype complexes of this series, compounds $[\text{Mn}_6(\mu_3\text{-O})_2(\text{O}_2\text{CR})_2(\text{salox})_6(\text{R}'\text{OH})_4]$ ($\text{R} = \text{Me}$, Ph ; $\text{R}' = \text{Et}$). Investigation of the electron spin dynamics of **1** carried out by solid state ^1H NMR measurements, clearly revealed an energy gap of $\Delta/k_B = 20$ K between the ground and the first excited state. Magnetic susceptibility measurements from polycrystalline samples of **5** revealed the presence of antiferromagnetic interactions in the $[\text{Mn}_3^{\text{III}}]$ unit. The data were fitted in the 100–300 K range by considering only intra-unit exchange couplings and yielded $J = -11.8$ cm $^{-1}$, corresponding to an $S = 2$ ground state.

Appendix A. Supplementary data

CCDC 694623, 694624, 694625, 694626 and 694627 contain the supplementary crystallographic data for **1** · 6MeCN, **2** · 2Me $_2$ CO, **3** · MeOH · 0.5H $_2$ O, **4** · n MeCN and **5** · n Me $_2$ CO. These data can be obtained free of charge via <http://www.ccdc.cam.ac.uk/conts/retrieving.html>, or from the Cambridge Crystallographic Data Centre, 12 Union Road, Cambridge CB2 1EZ, UK; fax: (+44) 1223-336-033; or e-mail: deposit@ccdc.cam.ac.uk. Tables of selected bond distances and angles for **2** · 2Me $_2$ CO, **3** · MeOH · 0.5H $_2$ O and **5** · n Me $_2$ CO are also available. Supplementary data associated with this article can be found, in the online version, at [doi:10.1016/j.poly.2008.08.021](https://doi.org/10.1016/j.poly.2008.08.021).

References

- [1] (a) For some recent examples on manganese iron complexes see: P. Baran, R. Boča, I. Chakraborty, J. Giapintzakis, R. Herchel, Q. Huang, J.E. McGrady, R.G. Raptis, Y. Sanakis, A. Simopoulos, *Inorg. Chem.* 47 (2008) 645; (b) J. Ballmann, S. Dechert, E. Bill, U. Ryde, F. Meyer, *Inorg. Chem.* 47 (2008) 1586; (c) A. Mishra, W. Wernsdorfer, K.A. Abboud, G. Christou, *Chem. Commun.* (2005) 54; (d) A. Mishra, Y. Pushkar, J. Yano, V.K. Yachandra, W. Wernsdorfer, K.A. Abboud, G. Christou, *Inorg. Chem.* 47 (2008) 1940; (e) R. Tagore, R.H. Crabtree, G.W. Brudvig, *Inorg. Chem.* 47 (2008) 1815.
- [2] (a) For some recent examples see: A. Mishra, A.J. Tasiopoulos, W. Wernsdorfer, E.E. Moushi, B. Moulton, M.J. Zaworotko, K.A. Abboud, G. Christou, *Inorg. Chem.* 47 (2008) 4832; (b) V. Chandrasekhar, B. Murugesha Pandian, R. Boomishankar, A. Steiner, J.J. Vittal, A. Hourri, R. Clérac, *Inorg. Chem.* 47 (2008) 4918; (c) D. Li, R. Clérac, O. Roubeau, E. Harté, C. Mathonière, R. Le Bris, S.M. Holmes, *J. Am. Chem. Soc.* 130 (2008) 252;
- (d) X. Yang, R.A. Jones, W.-K. Wong, *Dalton Trans.* (2008) 1676; (e) I.S. Lee, Y.K. Chung, *Inorg. Chem. Commun.* 10 (2007) 593.
- [3] R.E.P. Winpenny, *J. Chem. Soc., Dalton Trans.* (2002) 1.
- [4] (a) As the most characteristic example of this approach we mention the replacement of the bridging carboxylato ligands in the $[\text{Mn}_{12}]$ family of complexes. See for example: P. Artus, C. Boskovic, J. Yoo, W.E. Streib, L.-C. Brunel, D.N. Hendrickson, G. Christou, *Inorg. Chem.* 40 (2001) 4199; (b) N.E. Chakov, W. Wernsdorfer, K.A. Abboud, D.N. Hendrickson, G. Christou, *J. Chem. Soc., Dalton Trans.* (2003) 2243; (c) J.M. Lim, Y. Do, J. Kim, *Eur. J. Inorg. Chem.* (2006) 711; (d) E. Coronado, A. Forment-Aliaga, A. Gaita-Ariño, C. Giménez-Saiz, F.M. Romero, W. Wernsdorfer, *Angew. Chem., Int. Ed.* 43 (2004) 6152.
- [5] (a) See for example: V. Marvaud, C. Decroix, A. Scullier, C. Guyard-Duhayon, J. Vaissermann, F. Gonnet, M. Verdagner, *Chem. Eur. J.* 9 (2003) 1677; (b) Z.-G. Gu, W. Liu, Q.-F. Yang, X.-H. Zhou, J.-L. Zuo, X.-Z. You, *Inorg. Chem.* 46 (2007) 3236; (c) A.J. Tasiopoulos, A. Vinslava, W. Wernsdorfer, A. Abboud, G. Christou, *Angew. Chem., Int. Ed.* 43 (2004) 2117; (d) M. Soler, E. Rumberger, K. Folting, D.N. Hendrickson, G. Christou, *Polyhedron* 20 (2001) 1365; (e) M. Soler, W. Wernsdorfer, K. Folting, M. Pink, G. Christou, *J. Am. Chem. Soc.* 126 (2004) 2156; (f) X. Ottenwaelder, J. Cano, Y. Journaux, E. Rivière, C. Brennan, M. Nierlich, R. Ruiz-García, *Angew. Chem., Int. Ed.* 43 (2004) 850.
- [6] (a) See for example: J.-P. Costes, F. Dahan, W. Wernsdorfer, *Inorg. Chem.* 45 (2006) 5; (b) J.-P. Costes, F. Nicodème, *Chem. Eur. J.* 8 (2002) 3442; (c) J.-P. Costes, F. Dahan, F. Nicodème, *Inorg. Chem.* 42 (2003) 6556; (d) L.K. Thompson, T.L. Kelly, L.N. Dawe, H. Grove, M.T. Lemaire, J.A.K. Howard, E.C. Spencer, C.J. Matthews, S.T. Onions, *Inorg. Chem.* 43 (2004) 7605; (e) S.K. Dey, L.K. Thompson, L.N. Dawe, *Chem. Commun.* (2006) 4967; (f) L.N. Dawe, L.K. Thompson, *Angew. Chem., Int. Ed.* 46 (2007) 7440.
- [7] (a) See for example: C.P. Raptopoulou, V. Tangoulis, E. Devlin, *Angew. Chem., Int. Ed.* 41 (2002) 2386; (b) A.K. Boudalis, C.P. Raptopoulou, B. Abarca, R. Ballesteros, M. Chadlaoui, J.-P. Tuchsagues, A. Terzis, *Angew. Chem., Int. Ed.* 45 (2006) 432; (c) C.P. Raptopoulou, V. Tangoulis, V. Psycharis, *Inorg. Chem.* 39 (2000) 4452.
- [8] (a) See for example: C.P. Raptopoulou, A.K. Boudalis, Y. Sanakis, V. Psycharis, J.M. Clemente-Juan, M. Fardis, G. Diamantopoulos, G. Papavassiliou, *Inorg. Chem.* 45 (2006) 2317; (b) A.K. Boudalis, B. Donnadieu, V. Nastopoulos, J.M. Clemente-Juan, A. Mari, Y. Sanakis, J.-P. Tuchsagues, S.P. Perlepes, *Angew. Chem., Int. Ed.* 43 (2004) 2266; (c) A.K. Boudalis, Y. Sanakis, J.M. Clemente-Juan, B. Donnadieu, V. Nastopoulos, A. Mari, Y. Coppel, J.-P. Tuchsagues, S.P. Perlepes, *Chem. Eur. J.* 14 (2008) 2514.
- [9] For a comprehensive review of our work see A.K. Boudalis, Y. Sanakis, C.P. Raptopoulou, V. Psycharis, A. Terzis, *Polyhedron* 25 (2006) 1391 and references 7–10 cited therein.
- [10] C.P. Raptopoulou, A.K. Boudalis, Y. Sanakis, V. Psycharis, *Polyhedron* 24 (2005) 711.
- [11] (a) A.K. Boudalis, V. Nastopoulos, A. Terzis, C.P. Raptopoulou, S.P. Perlepes, *Z. Naturforsch.* 56b (2001) 122; (b) C. Gkiomi, A.K. Boudalis, Y. Sanakis, L. Leondiadis, V. Psycharis, C.P. Raptopoulou, *Polyhedron* 27 (2008) 2315.
- [12] Th.C. Stamatatos, A.K. Boudalis, Y. Sanakis, C.P. Raptopoulou, *Inorg. Chem.* 45 (2006) 7372.
- [13] C.P. Raptopoulou, V. Psycharis, *Inorg. Chem. Commun.* 11 (2008) 1194.
- [14] C.J. Milios, C.P. Raptopoulou, A. Terzis, F. Lloret, R. Vicente, S.P. Perlepes, A. Escuer, *Angew. Chem., Int. Ed.* 43 (2004) 210.
- [15] J.B. Vincent, H.-R. Chang, K. Folting, J.C. Huffman, G. Christou, D.N. Hendrickson, *J. Am. Chem. Soc.* 109 (1987) 5703.
- [16] M.W. Wemple, H.-L. Tsai, S. Wang, J.P. Claude, W.E. Streib, J.C. Huffman, D.N. Hendrickson, G. Christou, *Inorg. Chem.* 35 (1996) 6437.
- [17] J.-M. Clemente-Juan, C. Mackiewicz, M. Verelst, F. Dahan, A. Bousseksou, Y. Sanakis, J.-P. Tuchsagues, *Inorg. Chem.* 41 (2002) 1478.
- [18] F. James, M. Roos, *Comput. Phys. Commun.* 10 (1975) 343.
- [19] E. Fukushima, S.B.W. Roeder, *Experimental Pulse NMR*, Addison Wesley, Reading, MA, 1981.
- [20] S. Parsons, M. Murie, R. Winpenny, P. Wood, Private Communication to the CCDC, Code XAJVEK.
- [21] Rigaku/MSCCRYSTALCLEAR, Rigaku/MSI Inc., The Woodlands, Texas, USA, 2005.
- [22] G.M. Sheldrick, SHELXS-97: Structure Solving Program, University of Göttingen, Germany, 1997.
- [23] G.M. Sheldrick, SHELXL-97: Crystal Structure Refinement, University of Göttingen, Germany, 1997.
- [24] (a) For reviews see: G. Aromi, E.K. Brechin, *Struct. Bond.* 122 (2006) 1; (b) D. Gatteschi, R. Sessoli, *Angew. Chem., Int. Ed.* 42 (2003) 268; (c) G. Christou, D. Gatteschi, D.N. Hendrickson, R. Sessoli, *MRS Bull.* 25 (2000) 66.
- [25] (a) C.J. Milios, A. Vinslava, A.G. Whittaker, S. Parsons, W. Wernsdorfer, G. Christou, S.P. Perlepes, E.K. Brechin, *Inorg. Chem.* 45 (2006) 5272; (b) C.J. Milios, A. Vinslava, P.A. Wood, S. Parsons, W. Wernsdorfer, G. Christou, S.P. Perlepes, E.K. Brechin, *J. Am. Chem. Soc.* 129 (2007) 8; (c) C.J. Milios, A. Vinslava, W. Wernsdorfer, S. Moggach, S. Parsons, S.P. Perlepes, G. Christou, E.K. Brechin, *J. Am. Chem. Soc.* 129 (2007) 2754;

- (d) C.J. Milios, A. Vinslava, W. Wernsdorfer, A. Prescimone, P.A. Wood, S. Parsons, S.P. Perlepes, G. Christou, E.K. Brechin, *J. Am. Chem. Soc.* 129 (2007) 6547;
(e) C.J. Milios, R. Inglis, A. Vinslava, R. Bagai, W. Wernsdorfer, S. Parsons, S.P. Perlepes, G. Christou, E.K. Brechin, *J. Am. Chem. Soc.* 129 (2007) 12505.
- [26] P. Chaudhuri, *Coord. Chem. Rev.* 243 (2003) 143.
- [27] (a) J.M. Thorpe, R.L. Beddoes, D. Collison, C.D. Garner, M. Helliwell, J.M. Holmes, P.A. Tasker, *Angew. Chem., Int. Ed.* 38 (1999) 1119;
(b) P. Chaudhuri, M. Hess, E. Rentschler, T. Weyhermüller, U. Flörke, *New J. Chem.* (1998) 553;
(c) V. Zerbib, F. Robert, P. Gouzerh, *J. Chem. Soc., Chem. Commun.* (1994) 2179.
- [28] (a) Th.C. Stamatatos, D. Foguet-Albiol, C.C. Stoumpos, C.P. Raptopoulou, A. Terzis, W. Wernsdorfer, S.P. Perlepes, G. Christou, *J. Am. Chem. Soc.* 127 (2005) 15380;
(b) Th.C. Stamatatos, D. Foguet-Albiol, S.-C. Lee, C.C. Stoumpos, C.P. Raptopoulou, A. Terzis, W. Wernsdorfer, S.O. Hill, S.P. Perlepes, G. Christou, *J. Am. Chem. Soc.* 129 (2007) 9484.
- [29] (a) R. Wu, M. Poyraz, F.E. Sowrey, C.E. Anson, S. Wocadlo, A.K. Powell, U.A. Jayasooriya, R.D. Cannon, T. Nakamoto, M. Katada, H. Sano, *Inorg. Chem.* 37 (1998) 1913;
(b) J. An, Z.-D. Chen, J. Bian, X.-L. Jin, S.-X. Wang, G.-X. Xu, *Inorg. Chim. Acta* 287 (1999) 82;
(c) J. Li, S. Yang, F. Zhang, Z. Tang, S. Ma, Q. Shi, Q. Wu, Z. Huang, *Inorg. Chim. Acta* 294 (1999) 109;
- (d) A. Vlachos, V. Psycharis, C.P. Raptopoulou, N. Lalioti, Y. Sanakis, G. Diamantopoulos, M. Fardis, M. Karayanni, G. Papavassiliou, A. Terzis, *Inorg. Chim. Acta* 357 (2004) 3162;
(e) V. Psycharis, C.P. Raptopoulou, A.K. Boudalis, Y. Sanakis, M. Fardis, G. Diamantopoulos, G. Papavassiliou, *Eur. J. Inorg. Chem.* (2006) 3710.
- [30] P. Chaudhuri, E. Rentschler, F. Birkelbach, C. Krebs, E. Bill, T. Weyhermüller, U. Flörke, *Eur. J. Inorg. Chem.* (2003) 541.
- [31] (a) N.E. Chakov, L.N. Zakharov, A.L. Rheingold, K.A. Abboud, G. Christou, *Inorg. Chem.* 44 (2005) 4555;
(b) X. Xia, M. Verelst, J.-C. Daran, J.-P. Tuchagues, *J. Chem. Soc., Chem. Commun.* (1995) 2155.
- [32] C.J. Milios, P.A. Wood, S. Parsons, D. Foguet-Albiol, C. Lampropoulos, G. Christou, S.P. Perlepes, E.K. Brechin, *Inorg. Chim. Acta* 360 (2007) 3932.
- [33] (a) M. Fardis, G. Diamantopoulos, M. Karayianni, G. Papavassiliou, V. Tangoulis, A. Konsta, *Phys. Rev. B* 65 (2001) 014412;
(b) D. Procissi, B.J. Suh, A. Lascialfari, F. Borsa, A. Caneschi, A. Cornia, *J. Appl. Phys.* 91 (2002) 7173;
(c) M. Belesi, A. Lascialfari, D. Procissi, Z.H. Jang, F. Borsa, *Phys. Rev. B* 72 (2005) 014440.
- [34] G.E.G. Hardeman, N.J. Poulis, W.v.D. Lugt, *Physica (Utrecht)* 22 (1956) 48.
- [35] (a) T. Kohmoto, T. Goto, S. Maegawa, N. Fujiwara, Y. Fukuda, M. Kunitomo, M. Mekata, *Phys. Rev. B* 49 (1994) 6028;
(b) T. Goto, T. Koshiba, T. Kubo, K. Agawa, *Phys. Rev. B* 67 (2003) 104408.